Ru(bpy)₃²⁺/TiO₂-Codoped Zeolites: Synthesis, Characterization, and the Role of TiO₂ in Electron Transfer Photocatalysis

**Stefan H. Bossmann,*,† Claudia Turro,‡ Claudia Schnabel,† Megh Raj Pokhrel,†
Leon M. Payawan, Jr.,† Bodo Baumeister,† and Michael Wörner†**

*Lehrstuhl für Umweltmesstechnik, Universität Karlsruhe, 76128 Karlsruhe, Germany, and
Department of Chemistry, The Ohio State University, Columbus, Ohio 43210*

Received: July 12, 2000; In Final Form: March 16, 2001

Novel heterogeneous photocatalysts were developed which are able to transfer electrons from excited Ru(II) donors within the zeolite framework to Co(III) acceptor complexes in the exterior. The materials were prepared and characterized by elemental analysis, electrochemical methods, diffuse reflectance, and raster and transmission electron microscopy. The catalysts consist of zeolite Y-encapsulated Ru(bpy)₃²⁺ (bpy = 2,2′-bipyridine) sensitizers in close proximity to TiO₂ nanoparticles on the same support. The photophysical properties of Ru(bpy)₃²⁺ within the zeolite supercages were investigated at different loadings of Ru(bpy)₃²⁺ and TiO₂. The photoexcited MLCT state of the zeolite-entrapped Ru(bpy)₃²⁺ reacts via electron transfer with Co(dpphen)₃³⁺ (dpphen = 4,7-diphenyl-1,10-phenanthroline) in the exterior of the zeolite particles. The relative quenching of Ru(bpy)₃²⁺ by external Co(dpphen)₃³⁺ increases as the TiO₂ content within the zeolite is increased, where electron transfer from Ru(bpy)₃²⁺ complexes within the interior of the zeolite are able to transfer electrons to Co(dpphen)₃³⁺. This observation indicates that electrons can be transported from the interior of the zeolite to the surface in the presence of an appropriate electron relay, such as TiO₂ nanoparticles.

Introduction

The need to remove highly toxic compounds from potential sources of drinking water with efficient catalytic materials is of profound importance at the present time.[1−4] Thermal catalysts have been intensely investigated for this purpose; however, the reaction rates of such systems are slow compared to those possible with photoactivation. An advantage of photocatalysts is their reactivity at various temperatures, including 25 °C, whereas thermal catalysts typically require high temperatures for operation.[5,6] In addition, light-activated catalysts can be easily turned "on" or "off" in the presence or absence of a photon source, respectively. The most efficient heterogeneous photocatalysts to date consist of doped TiO₂, which requires ultraviolet light as an excitation source.[7,8] More efficient photocatalysts that operate with visible light are necessary to improve cost efficiency, to utilize solar energy, and to avoid the formation of highly toxic side products, such as dioxins, dibenzofurans, and polychlorinated hydrocarbons.[9−11]

Great attention has been given recently to the synthesis and characterization of zeolite-based catalysts for various applications.[9−12] The doping of zeolite Y with Ru(bpy)₃²⁺ (bpy = 2,2′-bipyridine) was initially reported in 1980 by DeWilde, Peeters, and Lunsford,[13] followed by extensive investigation of their physical and photophysical properties.[14−17] In general, the light-harvesting efficiency of zeolite-based photocatalysts containing Ru(bpy)₃²⁺ or related compounds as photosensitizers is found to be low if there are no electron relays embedded in their structural framework.[14−19] The presence of such electron relays is necessary since each Ru(II) complex is confined to a supercage. Therefore, an effective electron transport medium

is required for directed electron transfer and enhanced charge separation within the zeolite.[20] Until now, such an effective electron-transfer relay was missing in zeolite photocatalysis, and therefore, the possible applications of zeolitic systems were limited.

In an effort to improve the light harvesting and especially the electron-transfer efficiency of zeolite-photocatalysts, we synthesized zeolite Y-based systems that combine the sensitizer properties of Ru(bpy)₃²⁺ with the electron conducting properties of TiO₂ nanocrystals. The present work describes the synthesis of these materials, their characterization, and experiments toward the elucidation of their electron-transfer properties. In this design, it is expected that the TiO₂ nanocrystals within the zeolite framework will aid in the transport of electrons via their conduction band.[21] Furthermore, nearby TiO₂ nanoparticles can reduce photogenerated Ru(III) complexes, thus providing a closed Ru²⁺/³⁺ redox cycle regenerating the photoactive Ru(II) complex. On the basis of the observed electron transfer properties, we present a novel "Advanced Oxidation Process" (AOP), where these materials are able to use ultraviolet and visible light energy for photoenhanced electron transfer in aqueous media. An ultimate future goal of this work is the development of highly efficient heterogeneous photocatalysts for the decomposition of xenobiotics.

Experimental Section

General Procedures. All reagents and solvents used were of the highest purity available and were purchased from Aldrich and Fluka. H₂O possessed tridest. quality (UHQ-II). Co(dphen)₃³⁺ (dpphen = 4,7-diphenyl-1,10-phenanthroline) was prepared by a procedure previously reported.[22] X-ray powder diffractograms were recorded at the Institute for Mineralogy at the University of Karlsruhe (Prof. E. Althaus). Raster electron

---

* To whom correspondence should be addressed.
† University of Karlsruhe, Engler-Bunte-Institute.
‡ Ohio State University.

microscopy was performed in the laboratories for electron microscopy at the University of Karlsruhe (Prof. D. Gerthsen). For quantitative HPLC analysis, an HP Series II 1090 Liquid Chromatograph, equipped with a diode array detector and a LiChrospher-100 RP 18 column and precolumn, was used, where the mobile phase was 0.10 M (C$_2$H$_5$)$_3$N/H$_3$PO$_4$ (pH 7.0) and acetonitrile (65:35 v/v). TOC was measured by means of an Dohrmann DC-190 analyzer. We thank FISONS for elementary analysis (ICP/MS).

The program "IMAGE" was utilized (developed by the National Institute of Health, USA) for the analysis of the results of the raster electron microscopy. The program is able to identify and count particles of different size (TiO$_2$ surface nanoparticles and zeolite Y particles). Several in-house macros were written, which identified the size distribution of the TiO$_2$ particles. Using the size, the number per zeolite Y particle, and the average density of the TiO$_2$ particles ($d \approx 4.2$ g cm^{-3}),[23] we were able to estimate their amount on the surface of the zeolite.

All electrochemical experiments were performed using a computer controlled EG&G Princeton Applied Research potentiostat/Galvanostat (Model 263A) and the EG&G M270 software. Ru(bpy)$_3$Cl$_2$/Ru(bpy)$_3$(ClO$_4$)$_2$ was used as an electrochemical standard.[24] Cyclic voltammograms and differential pulse voltamograms (DPV, 50 mV pulse height) of the standard complex were taken using a glassy carbon working electrode versus SSCE reference electrode (sodium saturted calomel electrode) and a platinum sheet auxiliary electrode. For the measurements of the redox potentials of the Ru(bpy)$_3$$^{2+}$/TiO$_2$-codoped zeolites, a working electrode was constructed from a mixture of 200 mg of carbon paste (Metrohm) and 100 mg of doped or codoped zeolite powder. This mixture was pressed on both sides of a 15 mm × 15 mm gold grid. After immersion of this working electrode into 0.50 M Na$_2$SO$_4$ in water, the measurements were recorded (without ohmic drop correction). In control experiments, electrochemical signals due to the undoped zeolite Y composite electrode were identified (see Supporting Information, Figures S1−S4).

Steady-state and time-resolved fluorescence measurements were performed using an Edinburgh Analytical Instruments (EAI−FS/FL900) single-photon-counting instrument, which is able to fit lifetimes in the range of 500 ps to 500 μs. For these experiments, 10 mg of the zeolite samples was predried for 12 h at 100 °C, and then 3.0 mL H$_2$O was added prior to each measurement. For the quenching experiments, a Co(dpphen)$_3$$^{3+}$ stock solution was prepared in EtOH (0.1 mM) and added stepwise to the zeolite suspension containing the encapsulated luminescent *Ru(bpy)$_3$$^{2+}$ complex. Control experiments show that mixtures of various solvents with water, including ethanol, did not result in emission quenching of the Ru(bpy)$_3$$^{2+}$ encapsulated within the zeolite.

Synthesis of Zeolite-Entrapped Materials. *Ru(NH$_3$)$_{6-n-m}$-(H$_2$O)$_n$(AlO$^-$)$_m$]$^{2-m}$-Doped Zeolite Y.* A slurry of RuCl$_3$·H$_2$O (0.270−1.250 g, 1.198−5.54 mmol) in NH$_3$/H$_2$O (≥35% NH$_3$ per weight, 200 mL) was refluxed for 1 h. After cooling to room temperature, sodium-exchanged zeolite Y (Aldrich, 10.0 g, preheated at 200 °C for 2 h) was added in small portions. Concentrated NH$_3$ (300 mL) was then added dropwise, and the reaction mixture was refluxed again for 2 h. After cooling to room temperature, the white solid (with a pinkish cast) was filtered off and washed twice with H$_2$O (250 mL). Finally, the zeolite powder was dried over P$_2$O$_5$ under high vacuum (<10^{-7} Pa) for 48 h. Depending upon the quality of the filter used, the yields (calculated on the basis of zeolite employed) ranged from 95% to 98%.

Ru(bpy)$_3$$^{2+}$-Doped Zeolite Y. Slurries of Ru(NH$_3$)$_{6-n-m}$(H$_2$O)$_n$-(AlO$^-$)$_m$$^{2-m}$ (10.0 g) and 2,2′-bipyridine (0.60 g, 3.84 mmol) were refluxed for 3 h in a mixture of ethylene glycol (150 mL), DMSO (1 mL), and H$_2$O (1 mL). During the first hour, NH$_3$(g) was released from the boiling mixture. After cooling to room temperature, the orange-red solid was collected through filtration, washed twice with MeOH (250 mL), and then washed with 500 mL of a 2.0 M Na$_2$SO$_4$ solution. The solid product was finally washed twice with H$_2$O (250 mL), and the powder was then dried over P$_2$O$_5$ under high vacuum (<10^{-7} Pa) for 48 h. Depending upon the quality of the filters used, the yields ranged from 90% to 95%.

The content of Ru(bpy)$_3$$^{2+}$ within zeolite Y was determined by hydrolysis and HPLC analysis. The first hydrolysis procedure was adapted from that reported by Calzaferri and co-workers, where 25 mg of the Ru(bpy)$_3$$^{2+}$-doped zeolite Y material was stirred in 1 mL of 10% HF aqueous solution in the dark for 1 h.[25] After addition of 10 mL H$_2$O, the pH was adjusted to 7.0 with 4 M NaOH. The total volume of the solution was 20 mL after further dilution with H$_2$O. The second hydrolysis procedure consisted of the addition of 1 mL of concentrated H$_2$SO$_4$ (100%) to 25 mg of the Ru(bpy)$_3$$^{2+}$-doped zeolite Y materials and stirring in the dark for 24 h, followed by neutralization to pH 7.0 and dilution to a total volume of 20 mL. The solutions were filtered using 0.22 μm nylon filters (Roth) and injected into the HPLC. The typical retention time of Ru(bpy)$_3$$^{2+}$ was 4.11 ± 0.02 min, with a flow of 1.0 mL/min. Commercially available Ru(bpy)$_3$Cl$_2$ (Aldrich) was used for calibration.

Four other reaction products were found: Ru(bpy)$_2$(H$_2$O)$_2$$^{2+}$ (RT = 6.12 ± 0.02 min), Ru(bpy)$_2$(NH$_3$)$_2$$^{2+}$ (RT = 6.34 ± 0.04 min), and two unidentified products (RT = 7.02 ± 0.05 min, RT = 7.33 ± 0.06 min) featuring UV−vis absorption spectra similar to those of the identified bis-bipyridine ruthenium(II) complexes.[26] Ru(bpy)$_2$(H$_2$O)$_2$$^{2+}$ was independently prepared by treating Ru(bpy)$_2$Cl$_2$ with silver trifluoroacetic acid in DMF, and Ru(bpy)$_2$(NH$_3$)$_2$$^{2+}$ was synthesized by refluxing Ru(bpy)$_2$Cl$_2$ in concentrated NH$_3$/H$_2$O for 6 h. Both complexes were purified using descending column chromatography on Sephadex G-25 employing EtOH as an eluent. Both complexes were characterized after drying over P$_2$O$_5$ under high vacuum for 24 h by their typical UV−vis absorption spectra and their correct elemental (C, H, N) analyses. Note that Ru(bpy)$_2$(NH$_3$)(H$_2$O)$^{2+}$ (RT = 6.23 ± 0.02 min), which was synthesized by treating Ru(bpy)$_2$(H$_2$O)$_2$$^{2+}$ with 1.0 M NH$_3$/H$_2$O for 18 h, was not found among the identified reaction products.

Ru(bpy)$_3$$^{2+}$/TiO$_2$-Codoped Zeolite Y. Slurries of Ru(bpy)$_3$$^{2+}$-doped zeolite Y materials (10.0 g) in ethylene glycol (250 mL) were purged with argon for 1 h at −60 °C. Varying amounts of solid TiCl$_3$ were added in small portions to the mixture being actively stirred (vigorous reaction!). After warming to room temperature, the reddish suspension was stirred for 12 h. The reaction mixture was then opened to air and was stirred continuously for another 12 h. A saturated NaHCO$_3$ solution (150 mL) was added dropwise at 0 °C, and after all the CO$_2$ was released at that temperature, the reaction mixture was refluxed for 3 h. The red reaction product was filtered off and was subjected to three subsequent dispersion/filtration cycles employing H$_2$O (250 mL). Finally, the zeolite powder was heated for 1 h at 200 °C in an air atmosphere and was then stored over P$_2$O$_5$ under high vacuum (<10^{-7} Pa). Depending on the quality of the filters used, the yields ranged from 80% to 92%. TiO$_2$-doped zeolite Y was synthesized using the same experimental procedure starting with TiCl$_3$ and zeolite Y.

Results and Discussion

Synthesis of the Ru(bpy)₃²⁺-Containing Zeolite Y.
Ru(bpy)₃²⁺-Doped Zeolite Y. Zeolite Y belongs to the faujasite
family and is composed of tetrahedral SiO_4 and AlO_4^- building
blocks which form six-membered rings. The combination of
four- and six-membered rings leads to the formation of large
cavities, the β-cages. Zeolite Y, with chemical formula
$H_{500}Na_{56}Al_{56}Si_{136}O_{634}$, contains eight large cavities per unit
cell.[27] These supercages with diameter ~1.30 nm are connected
to each other by tunnels or "windows" of widest diameter ~0.74
nm. The ratio of cavities to windows in the interior of zeolite
Y is 1:3.

Since $Ru(bpy)_3^{2+}$ has a diameter of 1.08 nm,[28] its synthesis
must be performed using a "ship in a bottle" technique, where
the supercages of the zeolite Y are doped with Ru^{3+} and
subsequently the ligand 2,2′-bipyridine is added through the
windows of the zeolite structure. The Ru^{3+}/Na^+ ion exchange
was performed in NH_3/H_2O (30% per weight),[13] using $RuCl_3$
as the ruthenium source. Refluxing in NH_3/H_2O results in a
change in color from black to reddish-pink, which is indicative
of the reduction of Ru(III) to Ru(II).[14a] During this reaction,
the Ru(II) complexes $Ru(NH_3)_{6-n-m}(H_2O)_n(AlO^-)_m^{2-m}$ are
formed and are stabilized by the AlO^- groups of the zeolite,
which serve as the starting material for ligand exchange reactions
with 2,2′-bipyridine. Whereas previous procedures for the
synthesis of $Ru(bpy)_3^{2+}$ within the zeolite cavities attempted to
optimize the reaction by variation in temperature,[9] we dispersed
the zeolite Y particles in appropriate solvents, allowing definition
of the precise reaction temperature by their boiling temperatures
under normal pressure. This experimental procedure also results
in the best reproducibility and provides increased solubility of
the ligand, thus permitting its equal distribution among the
zeolite particles. In refluxing, ethanol (bp = 78 °C) $Ru(NH_3)_2$-
$(bpy)_2^{2+}$ is formed, whereas in boiling, ethylene glycol (bp =
196 °C) $Ru(bpy)_3^{2+}$ is prepared with very good yields (80–
95%). For technical reasons (filtration, recycling of the photo-
catalysts) relatively large zeolite particles were employed with
an average diameter of 1.0×10^{-6} m and an average number
of cavities per particle of $5 \pm 2 \times 10^8$.

TiO₂ Nanoparticles in Ru(bpy)₃²⁺-Doped Zeolite Y. The
procedure for the synthesis of TiO_2 nanoparticles within zeolites
consists of several steps shown in Scheme 1. The initial cation
exchange process is conducted with $TiCl_3$ as the titanium source
and ethylene glycol as the solvent.[29] An argon atmosphere is
imperative because of the risk of explosion if only traces of
oxygen are present! The hydrolysis of the titanium(III) chloride
on the zeolite particles was carried out at −5 to 0 °C, followed
by the oxidation of the Ti(III)/Ti(IV) clusters with air and
treatment at high temperature (150 °C) to obtain well-defined
Ti(IV) nanoparticles.

**Characterization of the Ru(bpy)₃²⁺/TiO₂-Codoped Zeolite
Y Materials.** *X-Ray Powder Diffraction.* The novel $Ru(bpy)_3^{2+}$/
TiO_2-codoped zeolite photocatalysts were characterized by X-ray
powder diffraction. All spectra obtained were consistent with
literature reports on zeolite Y.[30] No experimental evidence of
the X-ray pattern for crystalline $Ru(NH_3)_6^{2+}$, $Ru(bpy)_3^{2+}$, or
crystalline TiO_2 embedded in the zeolite Y structure is avail-
able.[31] From the X-ray powder diffraction pattern, it may be
concluded that neither the incorporation of $Ru(bpy)_3^{2+}$ nor the
subsequent incorporation of TiO_2 changes the framework of the
host (zeolite Y) significantly. The cavity of zeolite Y is
considerably larger (d = 1.38 nm) than the diameter of
$Ru(bpy)_3^{2+}$ (d = 1.08 nm), thus permitting many locations and
orientations of the ruthenium complex within the zeolite Y

**SCHEME 1: Synthesis of the Ru(bpy)₃²⁺/TiO₂-Codoped
Zeolite Y-Based Photocatalysts**
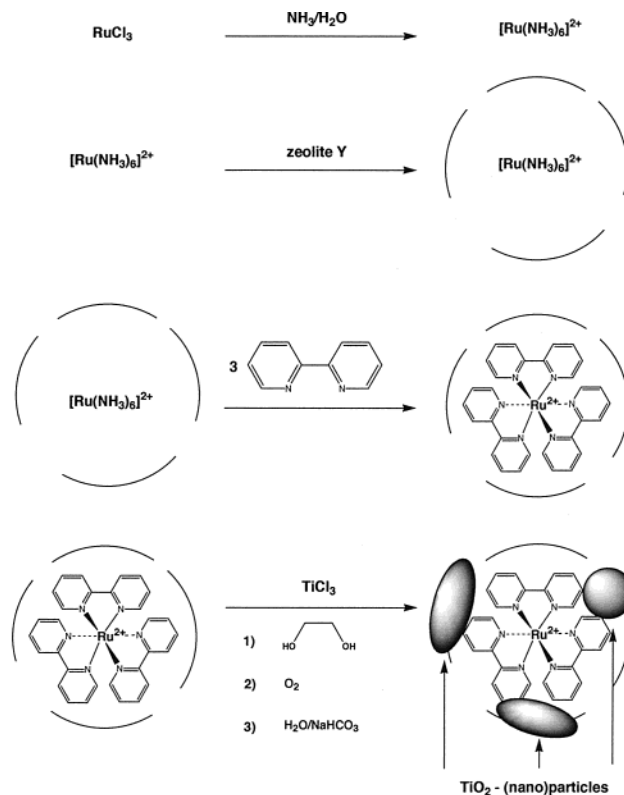
cavity. Therefore, no X-ray pattern arising from encapsulated
$Ru(bpy)_3^{2+}$ was observed. The powder diffraction data is not
consistent with the presence of any crystalline TiO_2; therefore,
we conclude that amorphous TiO_2 (nano)particles are formed
inside and/or on the outside of the zeolite particles.

HPLC Analysis of Ru(bpy)₃²⁺ Formed Within the Zeolite.
Upon dissolving the zeolite Y matrix in 10% HF as described
by Calzaferri and co-workers[25] or in concentrated H_2SO_4
followed by neutralization with aqueous NaOH, HPLC analysis
of the released complexes was made. Quantitative HPLC
showed that between 100% (low Ru(II) content) and >95%
(highest Ru(II) content) encapsulated $Ru(bpy)_3^{2+}$ was formed
during the synthesis. The presence of $Ru(bpy)_3^{2+}$ was confirmed
by comparison of the retention time of the released complex to
that of commercially available $Ru(bpy)_3Cl_2$ (Aldrich). The use
of concentrated H_2SO_4 led to slightly higher released $Ru(bpy)_3^{2+}$
than when employing HF. The amount of $Ru(bpy)_3^{2+}$ formed
during synthesis inside the zeolite cavities was remarkably
higher than previously reported[25] (Table 1 and Figure S1). In
employing ethylene glycol as solvent for 2,2′-bipyridine and
also for the dispersion of the zeolite Y particles and in employing
the DMSO-catalyzed reaction of the ligand with the Ru(II)
precursor complexes,[32] we achieved a more homogeneous
reaction system than that using the classic powder procedure
previously described. Our interpretation is supported by the
experimental observation by Calzaferri and co-workers, where
repeating the conventional synthetic (powder) procedure for a
second time led to the enhanced formation of the tris-homoleptic
sensitizer.[25] Furthermore, no evidence for the presence of Ru(III)
complexes was found.[33]

Raster Electron Microscopy. The structures of the $Ru(bpy)_3^{2+}$-
doped zeolite Y and $Ru(bpy)_3^{2+}$/TiO_2-codoped photocatalysts
were investigated using raster electron microscopy.[34] The six
images presented in Figure 1 are typical for all zeolite Y-based

Ru(bpy)$_3^{2+}$/TiO$_2$-Codoped Zeolites

J. Phys. Chem. B, Vol. 105, No. 23, 2001 **5377**

TABLE 1: Emission Lifetime(s) of Ru(bpy)$_3^{2+}$ in Zeolite Y Under Various Loadings of Ru(II) Complex and TiO$_2$

% Ru(bpy)$_3^{2+}$ ^{b,c}	% TiO$_2$ ^{a}	τ_1/ns	A^d	τ_2/ns	B^d
6 ± 0.3	0	412	96	54	4
12.5 ± 0.2	0	369	98	52	2
18 ± 0.2	0	283	87	60	12
23.5 ± 0.4	0	141	70	40	30
6 ± 0.3	9.5 ± 0.5	137	68	37	32
11 ± 0.4	9.5 ± 0.5	456	95	59	5
17.5 ± 0.3	9.5 ± 0.5	385	93	60	7
22 ± 0.5	9.5 ± 0.5	278	97	67	3
23 ± 0.5	12 ± 0.5	253	91	64	9
23 ± 0.5	15 ± 0.5	231	88	61	12
23 ± 0.5	17 ± 0.5	228	81	59	19
23 ± 0.5	19 ± 0.5	224	80	62	20
23 ± 0.5	22 ± 0.5	248	78	63	22
23 ± 0.5	24 ± 0.5	219	75	57	25
23 ± 0.5	27 ± 0.5	205	100		
23 ± 0.5	29 ± 0.5	217	100		
23 ± 0.5	31.5 ± 0.5	227	100		
23 ± 0.5	34.5 ± 0.5	266	100		
22 ± 0.5	37 ± 0.5	274	100		

^{a} Each data point results from three individual measurements ^{b} Percent by weight. ^{c} 25.1% loading represents one Ru(bpy)$_3^{2+}$ complex in each supercage. ^{d} Decays fit to [$A \exp(-t/\tau_1) + B \exp(-t/\tau_2)$]; the experimental error in the photophysical measurements is <±3 rel. %.

photocatalysts synthesized in this work and exhibit a smooth surface of the heterogeneous Ru(bpy)$_3^{2+}$-doped zeolite Y, which is covered with a increasing density of TiO$_2$ nanoparticles with increasing TiO$_2$ content. It is clear from the image that the structure of zeolite Y has not significantly changed during the doping with Ru(bpy)$_3^{2+}$. However, upon treatment of the Ru(bpy)$_3^{2+}$-doped zeolite Y with TiCl$_3$, the surface of the photocatalysts undergoes a remarkable change. After the TiO$_2$ doping procedure, nanoscopic TiO$_2$ particles are present at the surface. Their average diameter was determined to be in the $1 \times -5 \times 10^{-9}$ m range. A computer assisted analysis of the images using the program IMAGE led to the estimation that approximately 20% of the TiO$_2$ is located at the surface of the particles; therefore, 80% of the TiO$_2$ is embedded within the zeolite framework. According to the geometric features of zeolite Y and to the experimental fact that most of the cavities are filled with one Ru(bpy)$_3^{2+}$, we conclude that a significant fraction of the TiO$_2$ particles within the zeolite are located inside the zeolites' superstructure. However, this finding does not imply a distinct location of TiO$_2$ inside the Ru(bpy)$_3^{2+}$-doped zeolite Y, which is deposited during synthesis most likely at all accessible locations.

Transmission Electron Microscopy. The samples for the TEM measurement were prepared by embedding the particles in PMMA/C and cutting slices with a width of ~100 nm. These slices were then probed by TEM, showing black spots only where TiO$_2$ completely blocks the electron beam from the detector. A typical TEM image is shown in Figure 2. Although the resolution of the image is not optimal due to the intrinsic optical resolution of the instrument, we are able to conclude that TiO$_2$ nanoparticles possessing diameters <1.5 nm are symmetrically distributed within the zeolite's structure. Unfortunately, this method does not provide a quantitative measure of the TiO$_2$ content as a function of its location within the zeolite. However, these results show conclusively that TiO$_2$ is distributed throughout the doped zeolite Y particles investigated.

Electrochemical and Photophysical Measurements. *Electrochemistry.* The oxidation potential of the chloride salt of Ru(bpy)$_3^{2+}$, dissolved in 0.5 M Na$_2$SO$_4$, was measured to be 1.26$_5$ V versus SHE at a carbon paste/Au grid electrode, a value

consistent with those reported by others using conventional electrodes.[28] As shown in Table 2, when the complex is entrapped within the zeolite structure, there is a slight shift in the oxidation potential to 1.27$_6$ V versus SHE in the absence of TiO$_2$. Note that the electron transfer within the fully loaded zeolite Y is reversible. This finding is not consistent with the previously reported stabilization of the oxidized form of the complex, Ru(bpy)$_3^{3+}$, by the zeolite superstructure.[35] This effect is well established,[36] resulting in cathodic shifts of the redox potentials of many zeolite-encapsulated metal complexes.[37−39] However, our preparation methods of Ru(bpy)$_3^{2+}$-doped and especially of our novel Ru(bpy)$_3^{2+}$/ TiO$_2$-codoped zeolite Y materials are distinctly different from the previously reported procedures and lead to significantly higher Ru(bpy)$_3^{2+}$-contents as well a higher purity of Ru(bpy)$_3^{2+}$ inside the zeolite Y supercage.

An explanation for the reversible electron transfer of Ru(bpy)$_3^{2+}$ at high loadings in the presence as well as the absence TiO$_2$ within the zeolites framework is the supramolecular interaction of Ru(II) complexes occupying neighboring supercages. This finding is consistent with the theory developed by Dutta and Kincaid, which postulates a supramolecular interaction of Ru(bpy)$_3^{2+}$ complexes occupying neighboring supercages.[40] In several examples of strongly coupled metal−metal systems, an anodic shift of the oxidation potentials is indeed observed relative to the monomeric analogues, usually accompanied by an intervalence absorption band in the near-IR.[41−44] This behavior could be explained by the interaction of coupled redox centers which lead to the broadening of the electrochemical waves and, therefore, to a shift of the corresponding redox potentials.[45]

The doping procedure of the zeolites with titanium dioxide using TiCl$_3$ as titanium source, leads to an excess of protons in the interior of the zeolite's framework. Upon immersion in H$_2$O, a fraction of these protons generated during TiO$_2$ synthesis remain within the zeolite Y framework, most likely adsorbed onto the surface of the TiO$_2$ nanoparticles.

The electrochemical redox potentials measured by differential pulse voltammetry (DPV) are summarized in Table 2. Only redox potentials obtained for the first scan in the anodic direction of each electrochemical experiments are reported. However, when the DPV experiments are repeated several times, a systematic shift of the Ru(bpy)$_3^{2+/3+}$ redox potentials at high Ru(bpy)$_3^{2+/3+}$ loadings occurred. At the same time, the magnitudes of the electrochemical signals are diminishing consecutively. At a redox potential of approximately 1.24 V, the investigated sample, which was highly loaded with TiO$_2$ (37 ± 0.5%), was reduced to 50% of its original peak height.

Thus, we interpret our results as follows: In the beginning of the DPV experiments, residual traces of protons are present within the zeolite Y frameworks. Therefore, the typical cathodic shifts of the Ru(bpy)$_3^{2+}$ redox potentials were not detected during the first DPV scans if TiO$_2$ was present. The following systematic cathodic shifts down to 1.24 V (and even further) can be interpreted by the loss of intrazeolite protons due to the leaching process into the bulk electrolyte. Finally, the proton concentration inside the codoped zeolite Y becames too low to mediate extrazeolite electron-transfer processes. Consequently, the electrochemical waves of the Ru(bpy)$_3^{2+/3+}$ redox systems converge to zero. This behavior is consistent with the work reported by Ganesan and Ramaraj,[46] who also found that the zeolite Y framework does not support electron-transfer processes between Ru(bpy)$_3^{2+}$ metal complexes synthesized in its interior if the zeolite is immersed into aqueous 0.1 M Na$_2$SO$_4$. However,
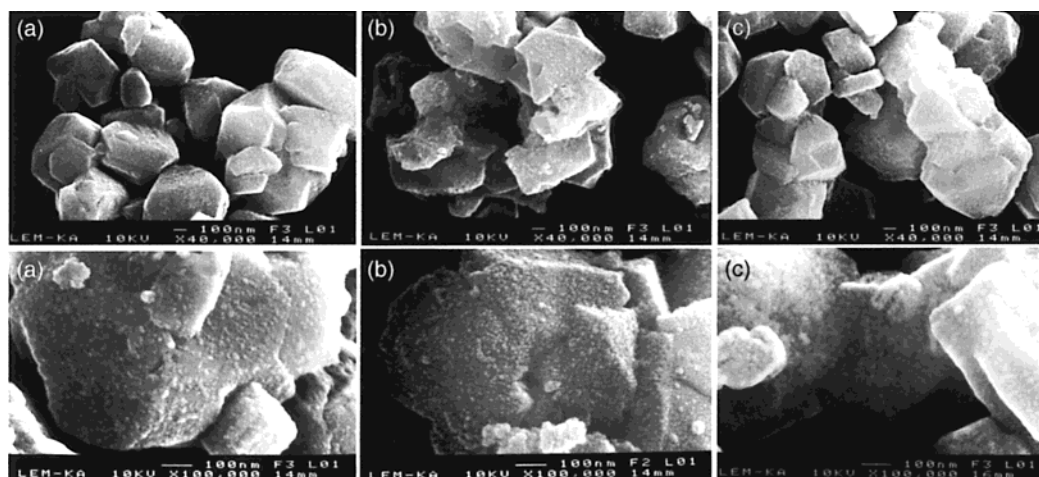
Figure 1. REM characterization of the novel materials. Two images possessing enlargement factors of 40 000 and 100 000 are shown: (a) zeolite Y (Ru(bpy)$_3^{2+}$ (23 ± 0.5%), TiO$_2$ (15 ± 0.5%), (b) zeolite Y (Ru(bpy)$_3^{2+}$ (23 ± 0.5%), TiO$_2$ (22 ± 0.5%)), and (c) Zeolite Y(Ru(bpy)$_3^{2+}$ (23 ± 0.5%), TiO$_2$ (27 ± 0.5%)).
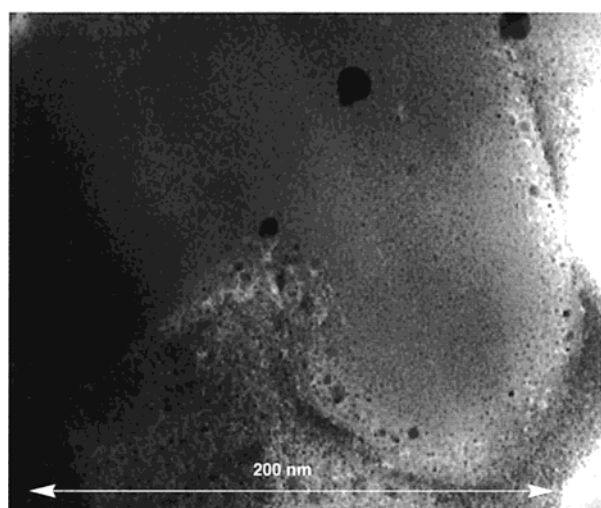
Figure 2. TEM characterization of a slice (thickness ≈ 100 nm) cut from a particle of Zeolite Y (Ru(bpy)$_3^{2+}$ (23 ± 0.5%)), TiO$_2$ (27 ± 0.5%)) embedded in PMMA/ graphite.

TABLE 2: Observed Redox Potentials (DPV experiments) of the Ru(III/II) Redox Couple of Ru(bpy)$_3^{2+}$ in Zeolite Y Under Various Loadings of Ru(II) Complex and TiO$_2$

% Ru(bpy)$_3^{2+}$ [a,b]	% TiO$_2$ [a]	$E^0_{Ru^{2+/3+}}$/V [c]	peak width at 50% peak height (mV)	peak current (μA)
23.5 ± 0.4	0	1.276 [d]	185	−1290
11 ± 0.4	9.5 ± 0.5	1.313 [e]	180	−280
22 ± 0.5	9.5 ± 0.5	1.327 [e]	153	−311
22 ± 0.5	37 ± 0.5	1.283 [d]	162	−1390
Ru(bpy)$_3^{2+}$ at C/Au-grid [f]	/	1.265 [d]	105	−305

[a] Percent by weight. [b] 25.1% loading represents one Ru(bpy)$_3^{2+}$ complex in each supercage. [c] Versus SHE. [d] Reversible electron transfer observed. [e] Virtually irreversible electron transfer observed in cathodic scan direction (DPV). $f_c = 2.54 \times 10^{-4}$ M.

if protons were provided by employing 0.05 M H$_2$SO$_4$ as the electrolyte solution, intense extrazeolite electron transfer between Ru(bpy)$_3^{2+}$ was observed.

Electronic Absorption and Emission. The diffuse reflectance spectra of zeolite Y prior to reaction, Ru(bpy)$_3^{2+}$-doped, and Ru(bpy)$_3^{2+}$/TiO$_2$-codoped zeolite Y are shown in Figure 4. As expected, no absorption in the 350 nm to 800 nm region is observed in the absence of metal complex and TiO$_2$ (Figure 4).

The characteristic MLCT absorption of Ru(bpy)$_3^{2+}$ from 400 to 500 nm is observed in the Ru(bpy)$_3^{2+}$-doped zeolite samples (Figure 4), with a maximum at 460 nm. This MLCT absorption maximum is red-shifted by 8 nm from that of Ru(bpy)$_3^{2+}$ in water, consistent with the shift in redox potential of the Ru(III/II) couple within the zeolite.[14b,47] It should be noted that the absorption spectra of the Ru(bpy)$_3^{2+}$-doped zeolites prepared by the method described here exhibit lower absorption at 530 nm, which corresponds to Ru(bpy)$_2$Cl$_2$ when compared to spectra of samples prepared by the dry method.[25]

It can be seen in Figure 4 that in the codoped Ru(bpy)$_3^{2+}$/ TiO$_2$ samples the absorption extends into the near-IR, Since TiO$_2$ itself does not absorb in the visible or near-IR regions of the spectrum, it may be concluded that there must be some interaction between the Ru(bpy)$_3^{2+}$ complexes encapsulated within the supercages and the TiO$_2$ nanoparticles located at the windows. Additional evidence of this interaction stems from the red shift of the absorption maximum of Ru(bpy)$_3^{2+}$ to 478 nm and the increased absorption of the Ru(bpy)$_3^{2+}$/TiO$_2$ systems throughout the 350−800 nm range relative to that in the absence of TiO$_2$.[25]

Although direct comparisons between the absorption and electrochemical results are desirable, the diffuse reflectance experiments only have a penetration depth of ~10 μm (from photoacoustic measurements).[48] In addition, we believe that the concentration of TiO$_2$ is greater near the surface than deeper within the zeolite particles, which are rectangular boxes with approximate dimensions of 1.0 × 0.5 × 0.5 μm^3.

The steady-state luminescence of Ru(bpy)$_3^{2+}$-doped zeolite samples is also red-shifted (λ_{em} ~ 630 nm) compared to that of the complex in solution ($\lambda_{em} \approx$ 610 nm). This behavior is in agreement with earlier findings.[40] The emission maximum further shifts to 645 nm in the Ru(bpy)$_3^{2+}$/TiO$_2$-codoped systems, consistent with a Ru(bpy)$_3^{2+}$−TiO$_2$ interaction. Owing to the limited light penetration and TiO$_2$ concentration gradient within the zeolite, quantitative comparisons are not possible.

Emission Lifetimes. The lifetimes of Ru(bpy)$_3^{2+}$-doped zeolite Y differ both with Ru(bpy)$_3^{2+}$ loading and TiO$_2$ content. The lifetimes and preexponential factors of various Ru(bpy)$_3^{2+}$− zeolite samples fit to a biexponential decay are listed in Table 1. The lifetimes and their corresponding contribution to the emission in the absence of TiO$_2$ show a decrease of the lifetime of the long-lived component and its relative intensity as Ru(bpy)$_3^{2+}$ loading increases. The biexponential decay of

Ru(bpy)$_3^{2+}$/TiO$_2$-Codoped Zeolites

J. Phys. Chem. B, Vol. 105, No. 23, 2001 **5379**
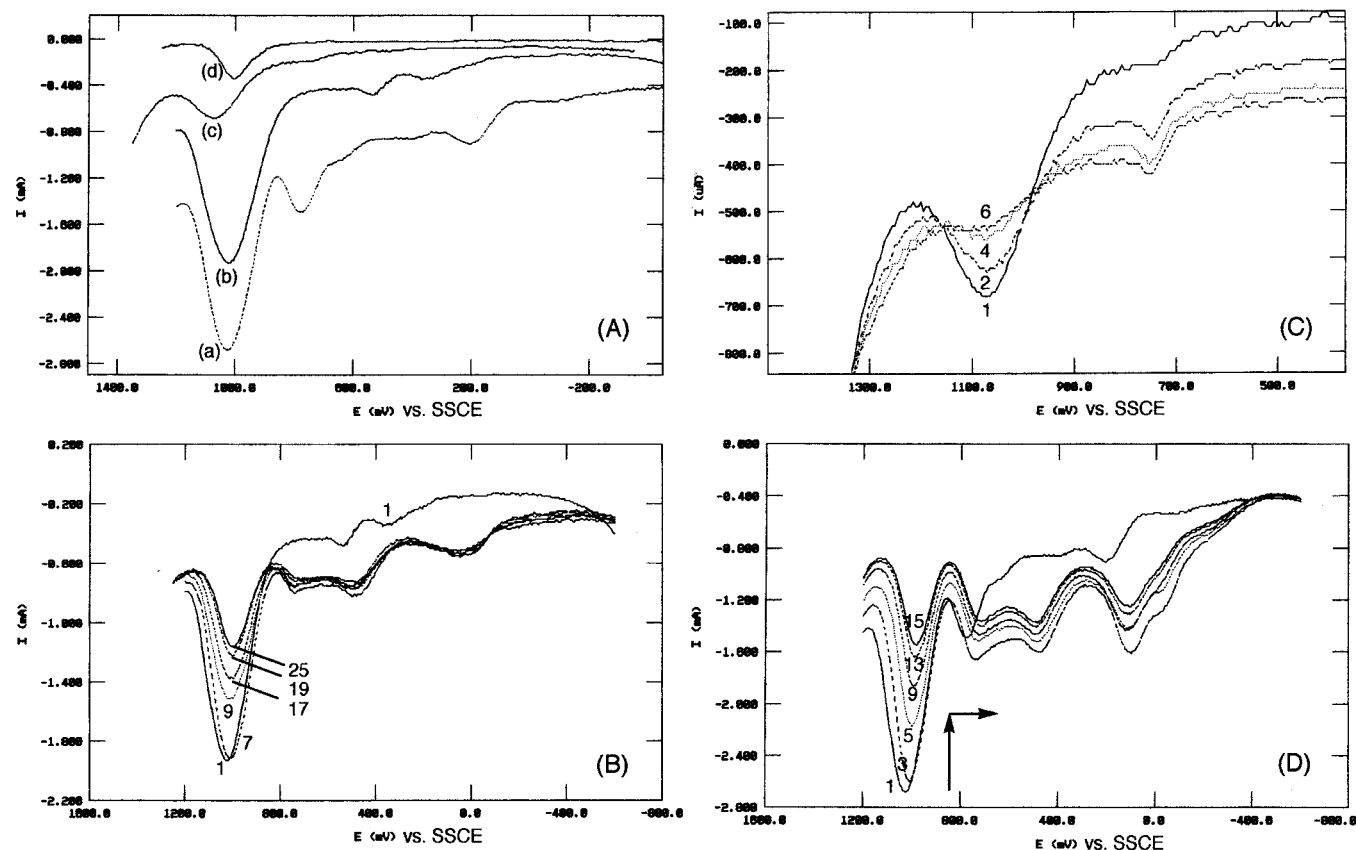
Figure 3. Overlay of differential pulse voltammograms (DPV, +50 mV pulse height, 10 mV s^{-1} scan rate). The measurements were recorded immediately after immersion of the working electrode into 0.50 M Na$_2$SO$_4$ in water. The numbers of the showed runs are indicated in the figures. (A) DPV measurements; first scans in the anodic direction of each electrochemical experiments are reported. (a) Zeolite Y containing 23 ± 0.5% (weight percent) of Ru(bpy)$_3^{2+}$ and 0% of TiO$_2$. (b) Zeolite Y containing 22 ± 0.5% (weight percent) of Ru(bpy)$_3^{2+}$ and 37 ± 0.5% of TiO$_2$. (c) Zeolite Y containing 11 ± 0.4% (weight percent) of Ru(bpy)$_3^{2+}$ and 9.5 ± 0.5% of TiO$_2$. Experiments a−c were performed employing a mixture of 200 mg carbon paste (Metrohm) and 100 mg of doped or codoped zeolite powder, pressed on both sides of a 15 mm × 15 mm gold grid as working electrode. (d) Ru(bpy)$_3^{2+}$ in 0.50 M Na$_2$SO$_4$ in water using a 15 mm × 30 mm gold grid/carbon paste/zeolite Y as working electrode. (B) DPV measurements of zeolite Y containing 23 ± 0.5% (weight percent) of Ru(bpy)$_3^{2+}$ and 0% of TiO$_2$. The first eight scans each in the anodic as well as the cathodic direction resulted in stable signals, a consecutive decrease of the DPV-signals is found starting with scan 9. (C) DPV measurements of zeolite Y containing 11 ± 0.4% (weight percent) of Ru(bpy)$_3^{2+}$ and 9.5 ± 0.5% of TiO$_2$. The recorded signals decrease beginning from the first scan consecutively. (D) DPV measurements of zeolite Y containing 22 ± 0.5% (weight percent) of Ru(bpy)$_3^{2+}$ and 37 ± 0.5% of TiO$_2$. The recorded signals decrease beginning from the first scan consecutively.
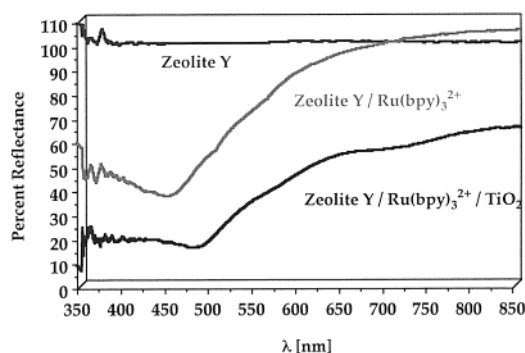
Figure 4. Diffuse reflectance spectra of (a) zeolite Y (Ru(bpy)$_3^{2+}$ (0%), TiO$_2$ (0%)), (b) Ru(bpy)$_3^{2+}$-doped zeolite Y (Ru(bpy)$_3^{2+}$ (23 ± 0.5%), TiO$_2$ (0%)), and (c) Ru(bpy)$_3^{2+}$/TiO$_2$-codoped zeolite Y (Ru(bpy)$_3^{2+}$ (23 ± 0.5%), TiO$_2$ (27 ± 0.5%)).

Ru(bpy)$_3^{2+}$ encapsulated within the zeolite Y supercages has been previously reported and discussed in detail, where the two lifetime components were attributed to complexes residing in different locations within the zeolite supercages.[16] However, as it becomes clear from Table 1, the relative contribution of the minor luminescent component increases with increased loadings of zeolite-entrapped Ru(bpy)$_3^{2+}$. If different locations of

Ru(bpy)$_3^{2+}$ within the zeolite Y supercage would be responsible for the occurrence of a second lifetime component, the relative contribution of the short-lived component (B) should not change. Therefore, the observed behavior is consistent with the theory developed by Dutta, Kincaid, and co-workers,[40] which attributed the minor luminescence components to Ru(bpy)$_3^{2+}$ complexes occupying neighboring supercages.

In codoped Ru(bpy)$_3^{2+}$/TiO$_2$ zeolite Y, the observed decay is strongly dependent on TiO$_2$ loading (Table 1). However, this does not imply a simple or even linear dependency of the observed emission lifetimes on the TiO$_2$ content. At low TiO$_2$ concentrations, the decay remains biexponential. However, above 27 ± 0.5% TiO$_2$ loading, the emission lifetime becomes monoexponential and increases with TiO$_2$ concentration.

As of yet, we could not discern all of the factors contributing to the observed complicated emission behavior of the zeolite Y embedded Ru(bpy)$_3^{2+}$* as a function of the TiO$_2$ loading. However, two major contributing factors could be identified from the literature: (1) H$_2$O quenches the excited MLCT state of ruthenium(II)-polypyridyl complexes.[28] The synthesis of TiO$_2$ inside the zeolites superstructure decreases the water content of the zeolite due to the space (and adsorption site) consumption by TiO$_2$. Therefore, the luminescence lifetime of zeolite Y-embedded Ru(bpy)$_3^{2+}$ should increase if the TiO$_2$ content

increases. (2) Since TiO$_2$ is known to quench the Ru(bpy)$_3^{2+}$ excited state,[29] the observed emission stems only from Ru(II) complexes that are not in direct proximity to TiO$_2$. Steady-state experiments show that those Ru(bpy)$_3^{2+}$ complexes located near TiO$_2$ within the zeolite do not emit light, since the emission intensity decreases dramatically while the lifetime remains constant or increases with added TiO$_2$. These observations are consistent with static quenching being the only operative quenching mechanism of the Ru(bpy)$_3^{2+}$ excited state by TiO$_2$. The increase in the lifetime observed as well as the change from a bisexponential luminescence decay to a monoexponential decay pattern as more TiO$_2$ is added to the zeolite is due to the presence of less accessible space in the supercages, resulting in lower Ru(bpy)$_3^{2+}$ mobility.

Finally, the precipitation of amorphous TiO$_2$ in the interior of zeolite Y must be regarded as a statistical process. Therefore, amorphous TiO$_2$ particles may be present inside the zeolite Y's framework at various locations. It is known that the quenching of the Ru(bpy)$_3^{2+}$ excited state by TiO$_2$ is strongly dependent on the size of the TiO$_2$ (nano)particles, which act as electron-transfer quenchers.[9] These different statistical distributions of the formed amorphous TiO$_2$ (nano)particles in size and location may account for the complicated luminescence behavior summarized in Table 1. Note that this behavior is reproducible as the data from Table 1 result from three independent experiments (synthesis of Ru(bpy)$_3^{2+}$/TiO$_2$-codoped zeolite Y, followed by the lifetime measurement).

Note that the luminescence behavior of zeolite Y possessing 6 $\pm$ 0.3% of Ru(bpy)$_3^{2+}$ and 9.5 $\pm$ 0,5% of TiO$_2$ is different from all other investigated samples and obviously does not fit in the theories presented here for the Ru(bpy)$_3^{2+}$/TiO$_2$-codoped zeolite Y photocatalysts. This sample is very low in its Ru(bpy)$_3^{2+}$ as well as its TiO$_2$ content. We hypothesize that the protons formed during TiCl$_3$ hydrolysis lead to the ion exchange Na$^+$ versus H$^+$ and that the strongly polar SiOH groups are formed, which are able to quench Ru(bpy)$_3^{2+}$*. At higher loadings, more sodium ions are exchanged versus Ru^{3+} and Ti^{3+} already during synthesis, and therefore, the quenching effect by SiOH groups is suppressed.

Quenching by External Co(dpphen)$_3^{3+}$. The emission of *Ru(bpy)$_3^{2+}$ encapsulated within the zeolite supercages is statically quenched by Co(dpphen)$_3^{3+}$ ($E_{Co^{2+/3+}}^0 = +0.33$ V vs SHE) on the exterior of the particles.[22,49] As the Co(dpphen)$_3^{3+}$ concentration is increased, the relative emission intensity of the Ru(II) complex decreases and finally reaches a plateau (Figure 5). From this behavior, we conclude that only the Ru(bpy)$_3^{2+}$ molecules residing near the zeolite's surface are quenched by the Co(III) complex. This observation is consistent with previous reports.[50,51] Since a short-lifetime component due to quenched Ru(bpy)$_3^{2+}$ is not observed within the 500 ps time resolution of the single-photon counting instrument, it may be concluded that the electron-transfer rate constant from Ru(bpy)$_3^{2+}$* trapped near the zeolite's surface to Co(dpphen)$_3^{3+}$ is very fast ($>10^{10}$ s^{-1}). Such static quenching from Ru(bpy)$_3^{2+}$ entrapped near the surface is expected, since the surface of zeolite Y is negatively charged at pH $\sim$7.8, resulting in electrostatic binding by the cationic Co(dpphen)$_3^{3+}$ to the exterior of the particles.

The relative emission intensity quenching by external Co(dpphen)$_3^{3+}$ for similar Ru(bpy)$_3^{2+}$ loadings (22–23%) with increasing TiO$_2$ content is also shown in Figure 5. In addition, the values of I_0/I in the absence and the presence of 200 μM Co(dpphen)$_3^{3+}$ for each sample relative to that without TiO$_2$ are listed in Table 3. It is clear that the addition of TiO$_2$ alone
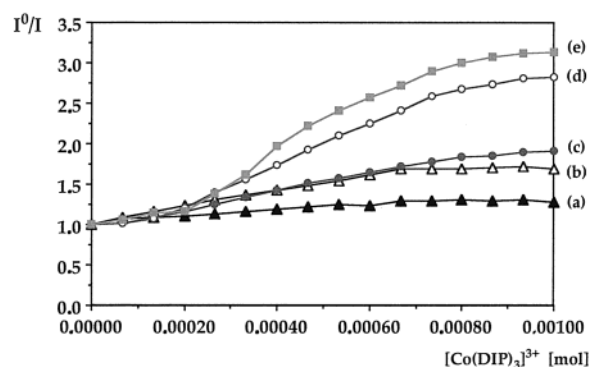
Figure 5. Relative emission intensity quenching by external Co-(dpphen)$_3^{3+}$ for similar Ru(bpy)$_3^{2+}$ loadings (22–23%) with increasing TiO$_2$ content. (a) Ru(bpy)$_3^{2+}$-doped zeolite Y (Ru(bpy)$_3^{2+}$ (23 $\pm$ 0.5%), TiO$_2$ (0%)), (b) Ru(bpy)$_3^{2+}$/TiO$_2$-codoped zeolite Y (Ru(bpy)$_3^{2+}$ (23 $\pm$ 0.5%), TiO$_2$ (17.$\pm$ 0.5%)), (c) Ru(bpy)$_3^{2+}$/TiO$_2$-codoped zeolite Y (Ru(bpy)$_3^{2+}$ (23 $\pm$ 0.5%), TiO$_2$ (27 $\pm$ 0.5%)), (d) Ru(bpy)$_3^{2+}$/TiO$_2$-codoped zeolite Y (Ru(bpy)$_3^{2+}$ (22 $\pm$ 0.5%), TiO$_2$ (31.5 $\pm$ 0.5%)), and (e) Ru(bpy)$_3^{2+}$/TiO$_2$-codoped zeolite Y (Ru(bpy)$_3^{2+}$ (22 $\pm$ 0.5%), TiO$_2$ (37 $\pm$ 0.5%)).

TABLE 3: Quenching of the Emission Intensity of Ru(bpy)$_3^{2+}$ (22.1 to 23.2%) in Zeolite Y in the Absence and Presence of 200 μM Co(dpphen)$_3^{3+}$ under Various Loadings of TiO$_2$

% Ru(bpy)$_3^{2+}$ [a,b]	% TiO$_2$ [a]	quenching[c] [Co] = 0 μM	quenching[c] [Co] = 200 μM calculated[d,e]	observed
23 $\pm$ 0.5	17 $\pm$ 0.5	1.56	1.90	2.25
23 $\pm$ 0.5	24 $\pm$ 0.5	1.68	2.05	2.37
23 $\pm$ 0.5	31.5 $\pm$ 0.5	1.89	2.30	4.15
22 $\pm$ 0.5	37 $\pm$ 0.5	2.71	3.31	4.55

[a] Percent by weight. [b] 25.1% loading represents one Ru(bpy)$_3^{2+}$ complex in each supercage. [c] From the integrated emission at each TiO$_2$ loading relative to 0% TiO$_2$ at 23.5% Ru(bpy)$_3^{2+}$ loading. [d] The emission intensity quenching by 200 μM Co(dpphen)$_3^{3+}$ in the absence of TiO$_2$ is I_0/I = 1.22. [e] Calculated by the division of the observed I_0/I values through the quenching of Ru(bpy)$_3^{2+}$* by TiO$_2$ (in the absence of Co(dpphen)$_3^{3+}$) at each % TiO$_2$ loading and multiplied by the quenching by 200 μM Co(dpphen)$_3^{3+}$ in the absence of TiO$_2$ (1.22).

increases the quenching of the emission intensity of Ru(bpy)$_3^{2+}$ entrapped within the zeolite supercages. Further decrease of the luminescence is observed upon addition of Co(dpphen)$_3^{3+}$ (Table 3). It is evident from the calculated and observed values in Table 3 that the quenching measured when both TiO$_2$ and Co(dpphen)$_3^{3+}$ are present is greater than that calculated assuming that each component quenches the Ru(bpy)$_3^{2+}$ emission independently from the other.

It may be concluded from these results that a greater fraction of the Ru(II) complexes is being quenched by a given concentration of Co(dpphen)$_3^{3+}$ in the exterior of the zeolite in the presence of TiO$_2$. This conclusion is consistent with the facilitation of electron transfer from Ru(bpy)$_3^{2+}$ in the interior of the zeolite to Co(dpphen)$_3^{3+}$ at the surface by encapsulated TiO$_2$. This increase in the electron-transfer rate with TiO$_2$ loading may be explained by the intervening TiO$_2$ nanoparticles providing a better coupling between donor and acceptor or acting as a direct electron relay. This explanation is consistent with the observed shifts in the redox potential, absorption, and emission of encapsulated Ru(bpy)$_3^{2+}$ in the presence of TiO$_2$ within the zeolite, clearly indicating a strong interaction between Ru(bpy)$_3^{2+}$* and TiO$_2$, which provides a communication pathway for Ru(bpy)$_3^{2+}$ molecules residing in adjacent supercages.

Ru(bpy)$_3^{2+}$/TiO$_2$-Codoped Zeolites

J. Phys. Chem. B, Vol. 105, No. 23, 2001 **5381**

Conclusion

The synthesis and characterization of a novel heterogeneous photocatalyst is reported. The catalyst consists of the sensitizer Ru(bpy)$_3^{2+}$ embedded in the cavity of zeolite Y in direct proximity to amorphous TiO$_2$ nanoparticles. The photophysical and electrochemical properties of Ru(bpy)$_3^{2+*}$ within the zeolite supercages were investigated. The photoexcited MLCT state of the zeolite-entrapped Ru(bpy)$_3^{2+}$ reacts via electron transfer with Co(dpphen)$_3^{3+}$ in the exterior of the zeolite particles. The relative quenching of Ru(bpy)$_3^{2+}$ by external Co(dpphen)$_3^{3+}$ increases as the TiO$_2$ content within the zeolite is increased, where electron transfer from Ru(bpy)$_3^{2+*}$ complexes within the interior of the zeolite are able to transfer electrons to external Co(dpphen)$_3^{3+}$. This observation indicates that electrons can be transferred from the interior of the zeolite to the surface in the presence of an appropriate electron relay, such as TiO$_2$ nanoparticles. This finding is of significant importance for the development of highly efficient AOT catalysts.

Supporting Information Available: Figures detailing HPLC analysis data, pulse voltammograms, DPV measurements, and redox potential. This material is available free of charge via the Internet at http://pubs.acs.org.

References and Notes

(1) (a) Legrini, O.; Oliveros, E.; Braun, A. M. *Chem. Rev.* **1993**, *93*, 671−698. (b) Göb, S.; Oliveros, E.; Bossmann, S. H.; Braun, A. M.; Guardani, R.; Nascimento, C. A. O. *Chem. Eng. Process.* **1999**, *38*, 373−382. (b) Alfano, O. M.; Bahnemann, D.; Cassano, A. E.; Dillert, R.; Goslich, R. *Catal. Today* **2000**, *58*, 199−230. (c) Pelitetti, E.; Minero, C.; Maurino, V. *Adv. Colloid Interface Sci.* **1990**, *32*, 271−316. (d) Bahnemann, D.; Cunningham, J.; Fox, M. A.; Pelizzetti, E.; Pichat, P.; Serpone, N. *Aquat. Surf. Photochem.* **1994**, 261−316.

(2) (a) Scaiano, J. C.; Garcia, H. *Acc. Chem. Res.* **1999**, *32*, 783−793. (b) Sanjuan, A.; Alvaro, M.; Aguirre, G.; Garcia, H.; Scaiano, J. C. *J. Am. Chem. Soc.* **1998**, *120*, 7351−7352.

(3) (a) Stafford, U.; Gray, K. A.; Kamat, P. V. *Heterog. Chem. Rev.* **1996**, *3*, 77−104. (b) Kamat, P. V.; Vinodgopal, K. *Mol. Supramol. Photochem.* **1998**, *2*, 307−350.

(4) (a) Andreozzi, R.; Caprio, V.; Insola, A.; Marotta, R. *Catal. Today* **1999**, *53*, 51−59. (b) Bauer, R.; Waldner, G.; Fallmann, H.; Hager, S.; Klare, M.; Krutzler, T.; Malato, S.; Maletzky, P. *Catal. Today* **1999**, *53*, 131−144.

(5) Barrow, G. M.; Herzog, G. W. *Physikalische Chemie; Teil III: Thermodynamische und kinetische Behandlung chemischer Reaktionen*; F. Vieweg & Sohn: Braunschweig, 1983; p 68−92.

(6) (a) Sanjuan, A.; Aguirre, G.; Alvaro, M.; Garcia, H.; Scaiano, J. C. *Appl. Catal., B* **2000**, *25*, 257−265. (b) Sanjuan, A.; Aguirre, G.; Alvaro, M.; Garcia, H. *Water Res.* **2000**, *34*, 320−326. (c) Sanjuan, A.; Alvaro, M.; Corma, A.; Garcia, H. *Chem. Commun.* **1999**, 1641−1642. (d) Sanjuan, A.; Aguirre, G.; Alvaro, M.; Garcia, H. *Appl. Catal., B* **1998**, *15*, 247−257. (e) Alvaro, M.; Garcia, H.; Sanjuan, A.; Espla, M. *Appl. Catal., A* **1998**, *175*, 105−112.

(7) Pichat, P.; Guillard, C.; Maillard, C.; Amalric, L.; D'Oliveira, J. *Trace Met. Environ.* **1993**, *3*, 207−223.

(8) (a) Ranjit, K. T.; Willner, I.; Bossmann, S. H.; Braun, A. M. *Res. Chem. Intermed.* **1999**, *25*, 733−756. (b) Ranjit, K. T.; Cohen, H.; Willner, I.; Bossmann, S. H.; Braun, A. M. *J. Mater. Sci.* **1999**, *34*, 5273−5280. (c) Ranjit, K. T.; Willner, I.; Bossmann, S. H.; Braun, A. M. *J. Phys. Chem. B* **1998**, *102*, 9397−9403.

(9) Bossmann, S. H. *Kombinierte photophysikalische, Elektronenspin-resonanz - und analytische Untersuchungen in mikroheterogenen und heterogenen Systemen als Grundlage der Entwicklung phänomenologischer und topologischer Modelle*; Universität Karlsruhe: Karlsruhe, 1997.

(10) Sanjuan, A.; Alvaro, M.; Corma, A.; Garcia, H. *Chem. Commun.* **1999**, 1641−1642.

(11) (a) Nasr, C.; Vinodgopal, K.; Fisher, L.; Hotchandani, S.; Chattopadhyay, A. K.; Kamat, P. V. *J. Phys. Chem.* **1996**, *100*, 8436−42. (b) Vinodgopal, K.; Wynkoop, D. E.; Kamat, P. V. *Environ. Sci. Technol.* **1996**, *30*, 1660−6.

(12) (a) Reschetilowski, W. *Zeolithische Molekularsiebe in der chemischen Technik*; DECHEMA: Frankfurt am Main, 1994; p 27. (b) Szostak, R. *Handbook of Molecular Sieves*; van Nostrand Reinhold: New York, 1992; p 183−227.

(13) DeWilde, W.; Peeters, G.; Lunsford, J. H. *J. Phys. Chem.* **1980**, *84*, 2306−10.

(14) (a) Dutta, P. K.; Turbeville, W. *J. Phys. Chem.* **1992**, *96*, 9410−9416. (b) Turbeville, W.; Robins, D. S.; Dutta, P. K. *J. Phys. Chem.* **1992**, *96*, 5024−9. (c) Borja, M.; Dutta, P. K. *Nature* **1993**, *362*, 43−45. (d) Dutta, P. K.; Borja, M. *J. Chem. Soc., Chem. Commun.* **1993**, *20*, 1568−1569. (e) Ledney, M.; Dutta, P. K. *J. Am. Chem. Soc.* **1995**, *117*, 7687−7691. (f) Das, S. K.; Dutta, P. K. *Langmuir* **1998**, *14*, 5121−5126. (g) Vitale, M.; Castagnola, N. B.; Ortins, N. J.; Brooke, J. A.; Vaidyalingam, A.; Dutta, P. K. *J. Phys. Chem. B* **1999**, *103*, 2408−2416.

(15) (a) Li, Z.; Mallouk, T. E. *J. Phys. Chem.* **1987**, *91*, 643−648. (b) Krueger, J. S.; Mayer, J. E.; Mallouk, T. E.; *J. Am. Chem. Soc.* **1988**, *110*, 8232−8234. (c) Rong, D.; Hong, H. G.; Kim, Y. I.; Krueger, J. S.; Mayer, J. E.; Mallouk, T. E. *Coord. Chem. Rev.* **1990**, *97*, 237−248. (d) Kim, Y. I.; Mallouk, T. E. *J. Phys. Chem.* **1992**, *96*, 2879−2885. (e) Yonemoto, E. H.; Kim, Y. I.; Schmehl, R. H.; Wallin, J. O.; Shoulders, B. A.; Richardson, B. R.; Haw, J. F.; Mallouk, T. E. *J. Am. Chem. Soc.* **1994**, *116*, 10557−63. (f) Kim, Y. I.; Keller, S. W.; Krueger, J. S.; Yonemoto, E. H.; Saupe, G. B.; Mallouk, T. E. *J. Phys. Chem. B* **1997**, *101*, 2491−2500.

(16) (a) Maruszewski, K.; Strommen, D. P.; Handrich, K.; Kincaid, J. R. *Inorg. Chem.* **1991**, *30*, 4579−4582. (b) Maruszewski, K.; Strommen, D. P.; Kincaid, J. R. *J. Am. Chem. Soc.* **1993**, *115*, 8345−50. (c) Maruszewski, K.; Kincaid, J. R. *Inorg. Chem.* **1995**, *34*, 2002−2006. (d) Sykora, M.; Kincaid, J. R. *Nature* **1997**, *387*, 162−164. (e) Szulbinski, W. S.; Kincaid, J. R. *Inorg. Chem.* **1998**, *37*, 859−864. (f) Sykora, M.; Maruszewski, K.; Treffert-Ziemelis, S. M.; Kincaid, J. R. *J. Am. Chem. Soc.* **1998**, *120*, 3490−3498. (g) Bhuiyan, A. A.; Kincaid, J. R. *Inorg. Chem.* **1999**, *38*, 4759−4764.

(17) Quayle, W. H.; Lunsford, J. H. *Inorg. Chem.* **1982**, *21*, 97−103.

(18) Senaratne, C.; Zhang, J.; Baker, M. D.; Bessel, C. A.; Rolison, D. R. *J. Phys. Chem.* **1996**, *100*, 5849.

(19) Ganesan, V.; Ramraj, R. *Langmuir* **1998**, *14*, 2497−2501.

(20) Dürr, H.; Bossmann, S. H.; Beuerlein, A. *J. Photochem. Photobiol., A* **1993**, *73*, 233−245.

(21) Memming, R. *Prog. Surf. Sci.* **1984**, *17*, 12−118.

(22) Ben-Avraham, D.; Schulman, L. S.; Bossmann, S. H.; Turro, C.; Turro, N. J. *J. Phys. Chem. B* **1998**, *102*, 5088−5093.

(23) Hollemann, A. F.; Wiberg, E.; Wiberg, N. *Lehrbuch der Anorganischen Chemie*; Walter de Gruyter: New York, 1985; p 1064.

(24) Bard, A. J.; Faulkner, L. R. *Electrochemical Methods: Fundamental and Applications*; Wiley: New York, 1980.

(25) Lainé, P.; Lanz, M.; Calzaferri, G. *Inorg. Chem.* **1996**, *35*, 3514−3518.

(26) Heppe, G. Thesis, University des Saarlandes, Saarbrücken, Germany, 1992.

(27) Suib, S. L. *Chem. Rev.* **1993**, *93*, 803.

(28) Juris, A.; Barigeletti, F.; Campagna, S.; Balzani, V.; Belser, P.; von Zelewsky, A. *Coord. Chem. Rev.* **1988**, *84*, 85−159.

(29) Kevan, L.; O'Reagan, B.; Kay, A.; Grätzel, M. *J. Electroanal. Chem.* **1993**, 291−297.

(30) Breck, D. W. *Zeolite Molecular Sieves*; Wiley: New York, 1974.

(31) Rilemma, D. P. R.; Jones, D. S.; Levy, H. A. *Chem. Commun.* **1979**, 849−852.

(32) Bossmann, S. H.; Ghatlia, N. D.; Turro, C.; Ottaviani, M. F.; Dürr, H.; Turro, N. J. *Synthesis* **1996**, *11*, 1313−1319.

(33) Verdonck, J. J.; Schoonheydt, R. A.; Jacobs, P. A. *J. Phys. Chem.* **1981**, *85*, 2393−2398.

(34) Bursill, L. A.; Lodge, E. A.; Thomas, J. M. *Nature* **1980**, *286*, 111.

(35) Briot, E.; Bedioui, F.; Balkus, K. J., Jr. *J. Electroanal. Chem.* **1998**, *454*, 83−89.

(36) Castro-Martins, S. D.; Khouzami, S.; Tuel, A.; Bentaarit, Y.; Murr, N. E.; Sellami, A. *J. Electroanal. Chem.* **1993**, *350*, 15−20.

(37) Bedioui, F.; Roué, L.; Briot, E.; Devynck, J.; Bell, S. L.; Balkus, K., Jr. *J. Electroanal. Chem.* **1994**, *373*, 19−29.

(38) Yoon, K. B. *Chem. Rev.* **1993**, *93*, 321−352.

(39) Vinod, M. P.; Das, T. K.; Chandwadkar, A. J.; Vijayamohanan, K.; Chandwadkar, J. G. *Mater. Chem. Phys.* **1999**, *58*, 37−43.

(40) Sykora, M.; Kincaid, J. R.; Dutta, P. K.; Castagnola, N. B. *J. Phys. Chem. B* **1999**, *103*, 309−320.

(41) (a) Baxter, P. N.; Lehn, J.-M.; Fischer, J.; Youinou, M.-T. *Angew. Chem., Int. Ed. Engl.* **1994**, *33*, 2284−2287. (b) Hanan, G. S.; Arana, C.

R.; Lehn, J.-M.; Fenske, D. *Angew. Chem., Int. Ed. Engl.* **1995**, *34*, 1122–1124. (c) Sleiman, H.; Baxter, P.; Lehn, J.-M.; Rissanen, K. *J. Chem. Soc., Chem. Commun.* **1995**, 715–716. (d) Hanan, G. S.; Arana, C. R.; Lehn, J.-M.; Baum, G.; Fenske, D. *Chem. Eur. J.* **1996**, *2*, 1292–1302.

(42) Kaifer, A. E.; Gómez-Kaifer, M. *Supramolecular Electrochemistry*; Wiley-VCH: Weinheim 1999; pp 164–179.

(43) Wang, Y.; Perez, W. J.; Zheng, G. Y.; Rillema, D. P.; Huber, C. L. *Inorg. Chem.* **1998**, *37*, 2227–2234.

(44) (a) Harriman, A.; Hissler, H.; Ziessel, R.; Cian, A. D.; Fischer, J. *J. Chem. Soc., Dalton Trans.* **1993**, 4067–4080. (b) Prospísil, L.; Heyrovsky, M.; Pecka, J.; Michl, J. *Langmuir* **1997**, *13*, 6294–6301.

(45) Wörner, M. Thesis, University of Hohenheim, Hohenheim, Germany, 1995.

(46) Ganesan, V.; Ramaraj, R. *Langmuir* **1998**, *14*, 2497–2501.

(47) (a) Incavo, J. A.; Dutta, P. K. *J. Phys. Chem.* **1990**, *94*, 3075–3081.

(48) Payawan, L. Thesis, University of Manila, Manila, The Philippines, 1999.

(49) Phenyl Rings of $Co(dpphen)_3^{2+}$ possess a van der Waals diameter of approximately 0.6 nm. The windows of zeolite Y have the widest diameter of approximately 0.74 nm. Adsorption constants of $Co(dpphen)_3^{2+}$ at the zeolite's surfaces are relatively weak (k approximately $450–500$ g^{-1}).

(50) Bessel, C. A.; Robinson, D. R. *J. Am. Chem. Soc.* **1997**, *119*, 12673–4.

(51) Yoon, K. B.; Park, Y. S.; Kochi, J. K. *J. Am. Chem. Soc.* **1996**, *118*, 12710–18.